RSC Advances

PAPER

View Article Online
View Journal | View Issue

Cite this: *RSC Adv.*, 2022, **12**, 2788

Probing the mechanism of the conversion of methyl levulinate into γ-valerolactone catalyzed by $Al(OiPr)_3$ in an alcohol solvent: a DFT study†

Zhaoyang Ju,[a] Shaokeng Feng,[a] Lanhui Ren,[b] Tingyu Lei,[c] Haixiang Cheng,[a] Mengting Yu*[a] and Chengsheng Ge*[a]

Received 17th November 2021
Accepted 6th January 2022

DOI: 10.1039/d1ra08429a

rsc.li/rsc-advances

Biomass-derived γ-valerolactone (GVL) is a versatile chemical that can be used in various fields. As an efficient, cheap, and sustainable catalyst, $Al(OiPr)_3$ has been successfully used in the conversion of methyl levulinate (ML) to GVL in the solvent isopropanol (IPA). However, the molecular mechanism of this conversion catalyzed by $Al(OiPr)_3$ remains ambiguous. To investigate the mechanism of the conversion of ML to GVL catalyzed by $Al(OiPr)_3$, the reaction pathways, including the transesterification, Meerwein–Ponndorf–Verley (MPV) hydrogenation, and ring-closure steps, were probed using density functional theory (DFT) calculations at the M062X-D3/def2-TZVP level. Among the elementary steps, it is found that ring-closure is the rate-determining step and that Al^{3+} can coordinate with the oxygen of 2-hydroxy-isopropyl levulinate (2HIPL) to catalyze the last ring-closure step. A four-centered transition state can be formed, and $Al(OiPr)_3$ shows a strong catalytic effect in the two steps of the ester exchange reaction. The center of $Al(OiPr)_3$ mainly coordinates with the carbonyl oxygen atom of the ester to catalyze the reaction. The present study provides some help in understanding the conversion mechanism of ML to GVL and designing more effective catalysts for use in biomass conversion chemistry.

1. Introduction

In light of environmental pollution and fossil resource depletion, lignocellulosic biomass has become a promising resource for the production of biofuels as a replacement for fossil fuels.[1,2] γ-Valerolactone (GVL) is accessible from lignocellulosic biomass,[3,4] and it has been identified as one of the most promising platforms for the sustainable production of fuels because of its outstanding physicochemical properties.[5] As an ideal precursor for the production of high-value chemicals to alleviate dependence on fossil fuels, GVL can be used to produce valuable chemicals such as dimethyl adipate, valeric esters, and long-chain alkanes, among others.[6–8] Furthermore, it could also be applied as an additive in food and drink because of its fruit flavour and low toxicity.[9,10]

Generally, GVL is yielded from the catalytic hydrogenation–cyclization of levulinic acid (LA) or its esters in an alcohol solvent. The traditionally used hydrogen donor is H_2, which requires high pressure to store and makes this process less safe.[11] Alcohol solvents are common and cheap reagents that exist in liquid state at room temperature. As an energy-saving and cost-effective method, catalytic transfer hydrogenation (CTH) in alcohol solvents is regarded as an attractive approach compared to traditional hydrogenation using high-pressure and flammable H_2.[12–15] As shown in Scheme 1, the production of GVL in alcohols usually involves transesterification, Meerwein–Ponndorf–Verley (MPV) reduction, and a ring-closure reaction to finish the overall process.[16,17] In particular, the use of secondary alcohols, such as isopropanol (i-PrOH) and 2-butanol, as a hydrogen donor has shown a better effect on MPV reduction.[18,19] According to the previous reports, several heterogeneous catalysts containing noble metals (Ru, Ir, Rh, Pd, Re, *etc.*) have been developed and have shown excellent abilities to yield GVL.[20–22] However, their high cost, difficult regeneration, and easy deactivation are highly challenging in practical applications.[23,24] Zhang *et al.*[25] reported that a 99.0% yield of GVL could be obtained from ethyl levulinate (EL) by using a ternary $Cu/ZnO/Al_2O_3$ catalyst in the CTH process with i-PrOH as the hydrogen donor. Moreover, He *et al.*[26] utilized a series of Al–Zr mixed oxides to obtain an 83.2% yield at 220 °C in 4 h using i-PrOH as the hydrogen donor, and reported that the acid–base sites played a synergic role in the production of GVL from EL. Recently, the noble metal-free catalyst $Al(OiPr)_3$ was shown to provide a high yield of GVL (up to 97.6%) under mild conditions (150 °C, 30 min); this catalyst has many advantages in the conversion of ML to GVL using i-PrOH as the solvent, such as its low price and easy availability.[18] The C–O bond of

[a]*College of Chemical & Material Engineering, Quzhou University, Quzhou 324000, China. E-mail: yumengting15@mails.ucas.edu.cn; gechengsheng@qzc.edu.cn*

[b]*Institute of Zhejiang University-Quzhou, Quzhou, 324000, China*

[c]*Institute of Coal Chemistry, Chinese Academy of Sciences, Taiyuan, 030001, China*

† Electronic supplementary information (ESI) available: *xyz* coordinates of all structures. See DOI: 10.1039/d1ra08429a

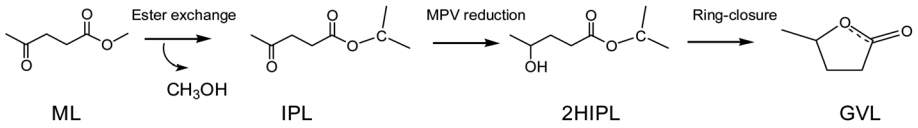

Scheme 1 A schematic representation of transesterification, hydrogenation, and ring-closure in the transformation of ML to GVL.

carboxylic acid derivatives could be activated by chiral Al^{3+}-based complexes, which also had a good effect on the MPV reduction.[27] Efficient catalytic processes are usually required for the hydrogenation of keto compounds in MPV reduction. The conversion of GVL on Al-based catalysts has been studied experimentally to achieve high yields, but the reaction mechanism still remains ambiguous. Therefore, it is also essential to understand the molecular reaction mechanism to provide some basic guidelines for the design of more efficient catalysts in the future. In the conversion of ML to GVL in i-PrOH, the ML undergoes transesterification, MPV hydrogenation, and ring-closure steps. In this work, we combined all these basic elements to probe the detailed reaction mechanism from ML to GVL catalyzed by $Al(OiPr)_3$. This will provide some help in understanding the mechanism of the conversion of ML to GVL from the viewpoint of theoretical calculations.

In this work, the detailed reaction mechanism of the conversion of ML into GVL catalyzed by $Al(OiPr)_3$ in i-PrOH has been carried out using DFT calculations at the M062X-D3/def2-TZVP level. In the conversion of ML into GVL, there are three main steps, namely, transesterification, the MPV reduction reaction, and ring-closure to finish the process. To explore the detailed reaction mechanism of the transformation of ML to GVL and the roles of $Al(OiPr)_3$ in the system, we have probed the conversion pathways of each step and studied the mechanism in the presence of $Al(OiPr)_3$. Finally, a detailed reaction mechanism has been proposed based on the DFT calculations. These results should provide a better understanding of the mechanism of the transformation of ML to GVL catalyzed by $Al(OiPr)_3$ in i-PrOH and give some basic guidelines to design more efficient catalysts.

2. Computational methods

All calculations were performed using the Gaussian 16 package,[28] and the geometric structures were generated using CYL view.[29] The geometry optimizations in this study were carried out using the M062X-D3 method[30,31] with the basis set def2-TZVP.[32] In the M062X-D3 method, the D3 term represents a dispersion correction.[33,34] Zhao *et al.* tested a series of the M06 suite of density functionals and recommended the M06-2X functional for applications involving thermochemistry and noncovalent interactions.[35] Def2-tzvp is the triple zeta valence basis set and has good quality for C, H, O, and Al, as has been reported in previous studies.[36,37] The harmonic vibrational frequencies of the reaction complexes were calculated at the same level of theory and used to first determine whether the optimized structures were true minima or transition states (TSs). To verify the transition states connecting the reactants with the appropriate products, the intrinsic reaction coordinates (IRCs) were also calculated using the algorithm developed by Gonzalez and Schlegel.[38] To account for the effects of the solution environment around the catalytic active site, the calculations were performed in an i-PrOH dielectric using the SMD solvation model[39] at the M06-2X-D3/def2-TZVP level for the geometry evaluation. The activation energy (G_a), which is the energy barrier, and the reaction energy (G_r) of the systems are defined as follows:

$$G_a = G_{TS} - G_R,\ G_r = G_p - G_R \quad (1)$$

where G_{TS}, G_R, and G_P represent the Gibbs free energies of the transition state, reactant, and product at 298.15 K and 100 kPa. To measure the reactive sites of the molecular surface, the electrostatic potential (ESP) of the reactants was analyzed and the standard Mulliken population analysis was used to obtain the charge density of each atom.[40,41]

3. Results and discussion

3.1 Transesterification reaction

The transesterification reaction is the main process to obtain some important energy sources, such as monoalkyl esters and glycerol, in alkyl alcohol.[42,43] In the conversion of ML to GVL in i-PrOH, the content of isopropyl levulinate (IPL) is relatively high in the early stage of the reaction, and then follows a decreasing trend at different temperatures of 110, 120, 130, and 140 °C within 60 min.[18] This indicates that the transesterification reaction of ML to IPL does indeed occur at the beginning of the transformation, and that the IPL would be further converted as the reaction proceeds. To investigate the reaction mechanism of the transesterification of ML to IPL in i-PrOH, the reaction pathways were probed using DFT calculations. As a useful tool to predict the reactive sites of a molecular surface, quantitative molecular surface analysis of ML, i-PrOH, and $Al(OiPr)_3$ was carried out, the results are shown in Fig. 1, in which blue-colored surfaces represent positive electrostatic potential and red-colored surfaces represent negative electrostatic potential. The negatively charged area is susceptible to attack by electrophilic reagents. In the structures of ML and i-PrOH, the negative electrostatic potential is mainly distributed around the oxygen atoms, with a less-positive charge around the methyl group. The Al^{3+} center of $Al(OiPr)_3$ can form strong H-bonds with the reactants. The differences in electrostatic potential play an important role in the formation of H-bonds to catalyze the reaction.

First, we probed the transesterification reaction of ML with i-PrOH as a model system without a catalyst (Ra → Pa), as shown

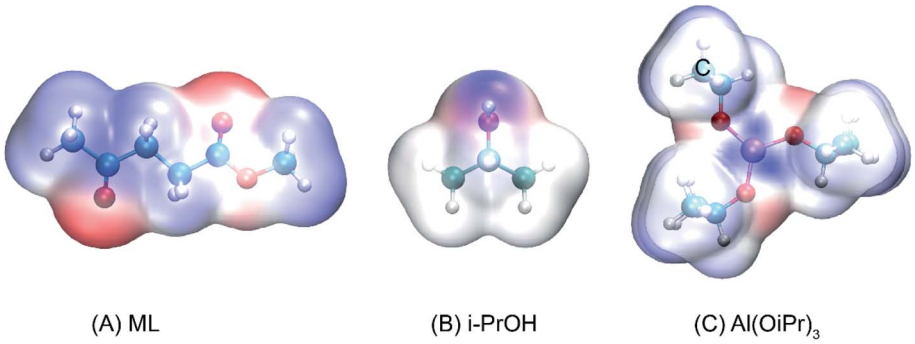

Fig. 1 Electrostatic potential surfaces of (A) ML, (B) i-PrOH, and (C) $Al(OiPr)_3$ (isovalue = 0.001 a.u.).

Table 1 Distance between the Al^{3+} center and the carboxyl oxygen atom of ML (R(Al–O)), the Mulliken charge densities of the carbonyl carbon ($q^{carbonyl\ C}$), and the negative frequencies of the TSs for the ester exchange step

	R(Al–O) [Å]	$q^{carbonyl\ C}$ [a.u.]	Negative frequency of TS [cm^{-1}]	Barrier [kcal mol^{-1}]
Uncatalyzed	—	0.3800	−1442.25	48.0
$Al(OiPr)_3$	1.874	0.0077	−1595.52	38.2

in Fig. 2. Initially, H-bonds can be formed between the oxygen (i-PrOH) and the carbon of the ester group (ML) with a distance of 2.818 Å. Then, a four-center cyclic TS is formed between i-PrOH and ML with distances of 1.649, 1.218, 1.205, 1.655 Å (C–O, O–H, H–O, and O–C), respectively. The geometry of TSa is illustrated in Fig. 2. Finally, i-PrOH will add to the ML to release methanol. The reaction barrier to complete the transesterification in i-PrOH was 48.0 kcal mol^{-1}, and this reaction is endothermic by 5.7 kcal mol^{-1}. The oxygen atom of i-PrOH acts as a nucleophile and attacks the carbonyl carbon atom of the ester molecule.

To investigate the reaction pathways catalyzed by $Al(OiPr)_3$, the reaction energies and optimized geometries of the reactant, TS, and product complexes were calculated, and are shown in Fig. 2 (Rb → Pb). The Al^{3+} of $Al(OiPr)_3$ mainly interacts with the oxygen of the ester group. A H-bond can be formed between $Al(OiPr)_3$ and ML with a distance of 1.873 Å. The oxygen of i-PrOH attacks the carbon of ester group. A four-center cyclic

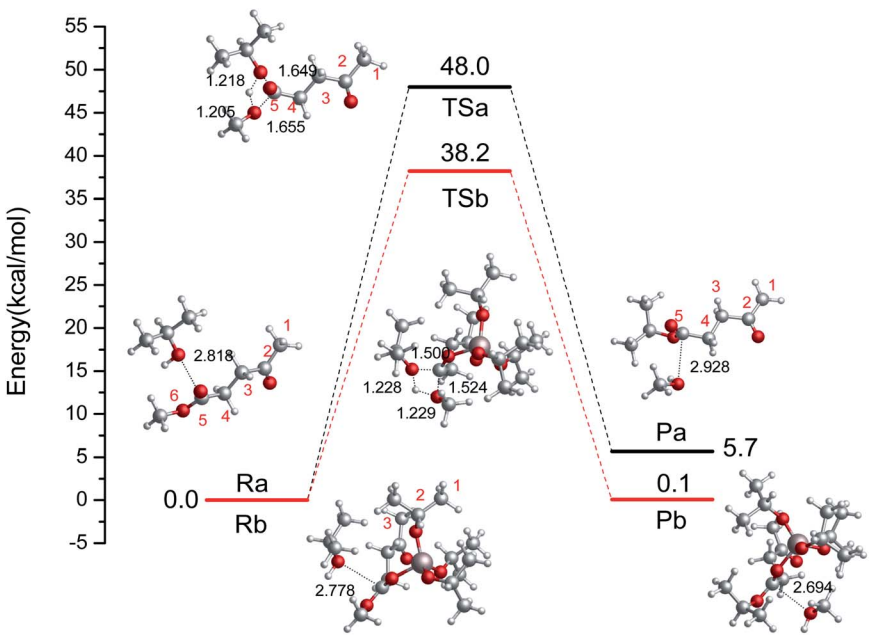

Fig. 2 The relative free energy diagram and optimized geometries of the reactants, TSs, and products without a catalyst (Ra–Pa) and with the catalyst $Al(OiPr)_3$ (Rb–Pb) (bond distances in angstroms).

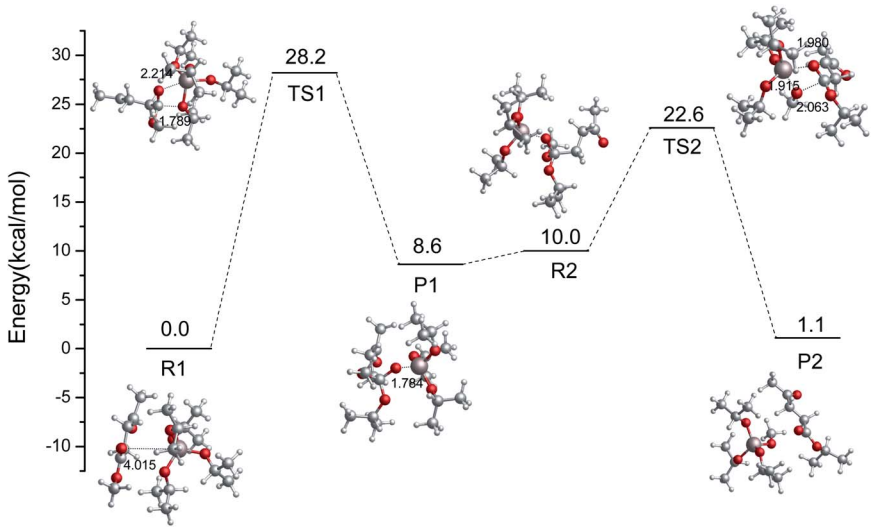

Fig. 3 Relative free energy diagram and optimized geometries for the ester exchange catalyzed by $Al(OiPr)_3$ *via* another pathway (bond distances in angstroms).

TSb structure is formed between i-PrOH and ML. This process is completed with a 38.8 kcal mol^{-1} energy barrier. This means that $Al(OiPr)_3$ exerts a catalytic effect to some extent by forming H-bonds with the oxygen of the ester group (ML). The R(Al–O) distance, Mulliken charges, and negative frequencies of the TS structures are listed in Table 1. The Mulliken charge of the carbonyl carbon ($q^{\text{carbonyl C}}$) in ML under $Al(OiPr)_3$ catalysis is 0.0077 a.u.; the decrease in the charge of the carbonyl carbon atom will be beneficial for the transesterification reaction.

In the imidazolium-IL-catalyzed isomerization of glucose to fructose, the imidazolium cations play the dual roles of H-bond donor and proton shuttle.[44] The role of Al^{3+}-based catalysts was shown to be shortening the proton transfer distance.[45] Similarly, another pathway catalyzed by $Al(OiPr)_3$ is also probed in this section. The relative energy scheme and optimized geometries of the reactant, TS, and product complexes are plotted in Fig. 3. Firstly, the Al^{3+} forms a strong H-bond with the oxygen of the ester group in ML, and then the i-$PrO^{\bullet}$ is added to the ester group carbon of ML. An intermediate (P1) is formed with a 28.2 kcal mol^{-1} energy barrier, and its formation is endothermic, with a reaction energy of 8.6 kcal mol^{-1}. Then, the $CH_3O^{\bullet}$ will be coordinated with the Al^{3+} to finish the transesterification in the second step (just opposite to the former process). The energy barrier of the second step to finish the transesterification is 12.6 kcal mol^{-1}, and this process is exothermic with a reaction energy of 8.9 kcal mol^{-1}. Comparing the energy barriers in these two kinds of transesterification catalyzed by $Al(OiPr)_3$ (Rb → Pb and R1 → P2), $Al(OiPr)_3$ plays a critical role in the second pathway (R1 → P2) to catalyze the transesterification. Additionally, the activation potential energy of the reaction catalyzed by $Al(OiPr)_3$ is much lower than that of the non-catalytic reaction, and $Al(OiPr)_3$ can indeed affect the transesterification reaction to decrease the energy barrier.

Table 2 Computed relative energies (kcal mol^{-1}) for the different hydrogen transfer reaction pathways in different ways and the negative frequencies of the TSs

	Activation energy [kcal mol^{-1}]	Reaction energy [kcal mol^{-1}]	Negative frequency of TS [cm^{-1}]
(A) Inter-	34.6	−0.2	−1453.74
(B) Intra-	51.0	−7.1	−812.46

3.2 Meerwein–Ponndorf–Verley (MPV) reduction

The catalytic hydrogenation of LA or its esters plays an important role in producing GVL with low energy consumption.[46] The Meerwein–Ponndorf–Verley (MPV) reaction is very selective toward the keto functional group, which offers the possibility of catalytic hydrogenation of biomass derivatives in the liquid phase.[17,47,48] In this section, we investigate the reaction pathways, including the energetics and structures, of the MPV hydrogenation of IPL to 2-hydroxy-isopropyl levulinate (2HIPL). To investigate the reaction barriers for the direct hydration of IPL using various hydrogen donors, we carried out computations without a catalyst. There are two pathways, *i.e.*, an inter- and an intra-molecular pathway, to achieve the hydrogenation. The free energies of the hydrogen transfer reactions and the negative frequencies of the TSs are summarized in Table 2. The hydrogen of i-PrOH is directly transferred through a six-membered ring TS structure (TSc). The IRCs were calculated to verify the TSs connecting the reactants with the appropriate products in this work. The IRCs (maxpoint = 100, stepsize = 10) corresponding to TSc in Fig. 4A are listed in Fig. S1.† Initially, H-bonds can form between the hydroxyl of i-PrOH and IPL, and then the protons transfer to IPL to produce 2HIPL and isopropanone. As shown in Fig. 4(A), the protons of hydroxyl and CH in i-PrOH transfer to the carbonyl of ML to complete the inter-molecular hydrogenation, and the energy barrier of inter-molecular hydrogenation is 51.0 kcal mol^{-1}. At the same time, IPL can undergo intra-molecular hydrogen transfer (Fig. 4(B)) to

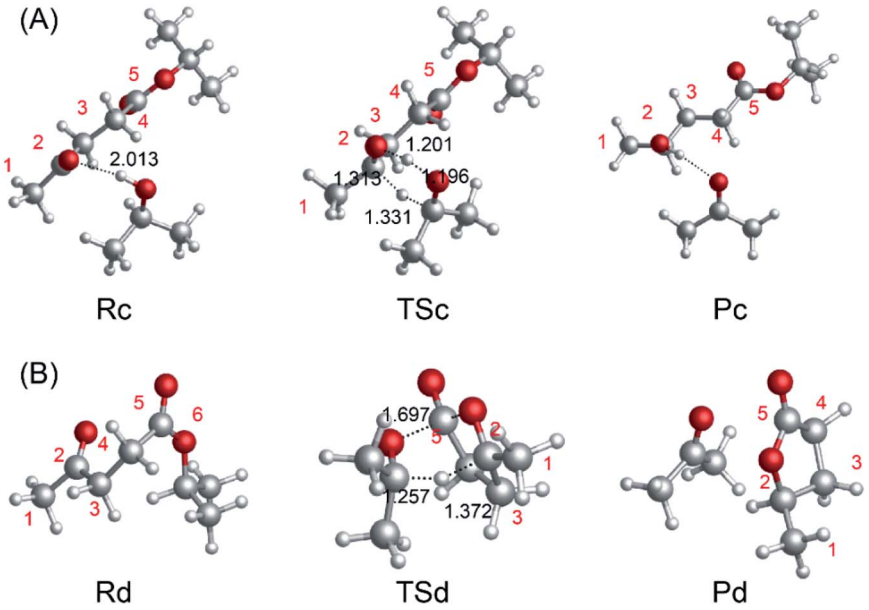

Fig. 4 (A) Intermolecular hydrogen transfer between IPL and i-PrOH to form 2HIPL and isopropanone. (B) Intramolecular hydrogen transfer involving IPL to form GVL and isopropanone.

form GVL and isopropanone. However, a barrier of 51.0 kcal mol^{-1} must be overcome in this process, and it is exothermic by 7.1 kcal mol^{-1}. The hydrogen donors can come from many sources, such as secondary alcohols or IPL. The energy barrier of inter-molecular hydrogenation is lower than that of intra-molecular hydrogenation. This further confirmed that the secondary alcohols are better than primary alcohols. The larger reaction barrier of intra-molecular hydrogenation implies that inter-molecular hydrogenation is preferred in the presence of hydrogen donors (solvents such as i-PrOH).

To investigate the pathways of the MPV reaction catalyzed by Al(OiPr)$_3$, the relative energies and the corresponding structures are shown in Fig. 5. Assary *et al.* reported the reaction pathways of MPV reduction catalyzed by Sn, Zr, and Al model catalysts.[49] The free energy of MPV hydrogenation from IPL to 2HIPL catalyzed by Al(OiPr)$_3$ at the MP2/6-311+G(3df, 3pd)//B3LYP/6-31+G(d)[49] and M06-2X-D3/def2-tzvp levels are compared in Fig. S2.† As shown in Fig. S2,† the activation barriers at the M06-2X-D3/def2-tzvp and MP2/6-311+G(3df,3pd)//B3LYP/6-31+G(d) level for the pathways reported by Assary *et al.* are less than 1 kcal mol^{-1}.[49] DFT-D3 provides a good description of π-stacking interactions for multiatomic systems.[50,51] The small difference in the energies is mainly caused by the structures optimized at the B3LYP and M06-2X-D3 levels, but both of them are reasonable to calculate the energies. Furthermore, Cohen *et al.* studied the mechanistic details of the MPV reduction of ketones *via* experiments and DFT calculations, and found that a six-membered ring TS is the most favorable pathway.[52]

Some similar reaction mechanisms for the MPV reaction of ketones catalyzed by Al(OiPr)$_3$ in i-PrOH solvent with a two-step

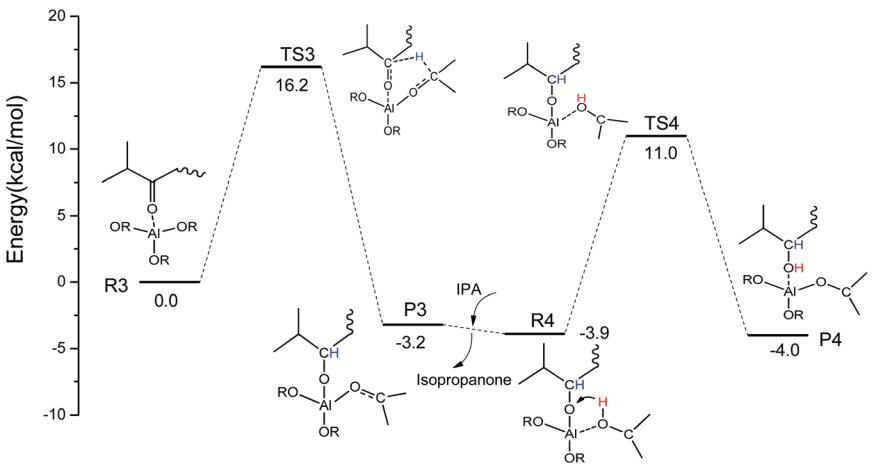

Fig. 5 The computed free energy profile with schematic diagrams of geometries for the hydrogenation of IPL to 2HIPL by Al(OiPr)$_3$ in i-PrOH medium (R=CH_3CHCH_3).

intermolecular hydrogen transfer mechanism were explored using DFT calculations. In the first step (R3 → P3), H-bonds are formed between $Al(OiPr)_3$ and the oxygen of the carbonyl group (IPL). The oxygen of the carbonyl group (IPL) can be activated by $Al(OiPr)_3$. Then, the hydrogen proton of C2 of $Al(OiPr)_3$ is transferred to the carbon of the carbonyl group (IPL) *via* a six-membered ring TS structure (TS3). This process requires an energy barrier of 16.2 kcal mol^{-1} to be overcome, and is exothermic by about 3.2 kcal mol^{-1}. The intermediate product P3 is formed to complete the first hydrogenation. In the solvent i-PrOH, isopropanone will be removed, and the second step (R4 → P4) will be continuous. The interaction position between $Al(OiPr)_3$ and IPL changes to form R4 due to the molecular flexibility. For the second hydrogenation of IPL (R4 → P4), the H of the hydroxyl of i-PrOH coordinated with Al^{3+} transfers to the O of the carbonyl group (IPL) *via* a six-membered ring TS structure (TS4). This process presents a 14.9 kcal mol^{-1} energy barrier to complete the MPV hydrogenation. The energy barrier of the first hydrogenation is a bit higher than that of the second. Additionally, a six-membered ring TS is formed between $Al(OiPr)_3$ and IPL in the MPV hydrogenation. The oxygen of IPL can be activated by coordination with $Al(OiPr)_3$.

3.3 Ring-closure step

To investigate the mechanism of the ring-closure step to give GVL, we probed the reaction pathway without a catalyst and those catalyzed by i-PrOH, 2HIPL, and H_2O. To compare the reactions catalyzed by the different catalysts quantitatively, the reaction of GVL and i-PrOH without any catalyst was first investigated and is shown in Fig. 6(A). To provide GVL, the O2 of 2HIPL approaches C5, and the H of the hydroxyl transfers to O6. The transition state involved in this process is TSe, in which the ester group C5–O6 bond (1.634 Å) is almost broken due to the attack of the oxygen of the hydroxyl with a C5–O2 distance of 1.726 Å. About 46.9 kcal mol^{-1} is required to cross the transition-state energy barrier. The reaction without a catalyst is an endothermic process of about 1.8 kcal mol^{-1}. In this process, catalysts such as i-PrOH, 2HIPL, and H_2O can participate in the

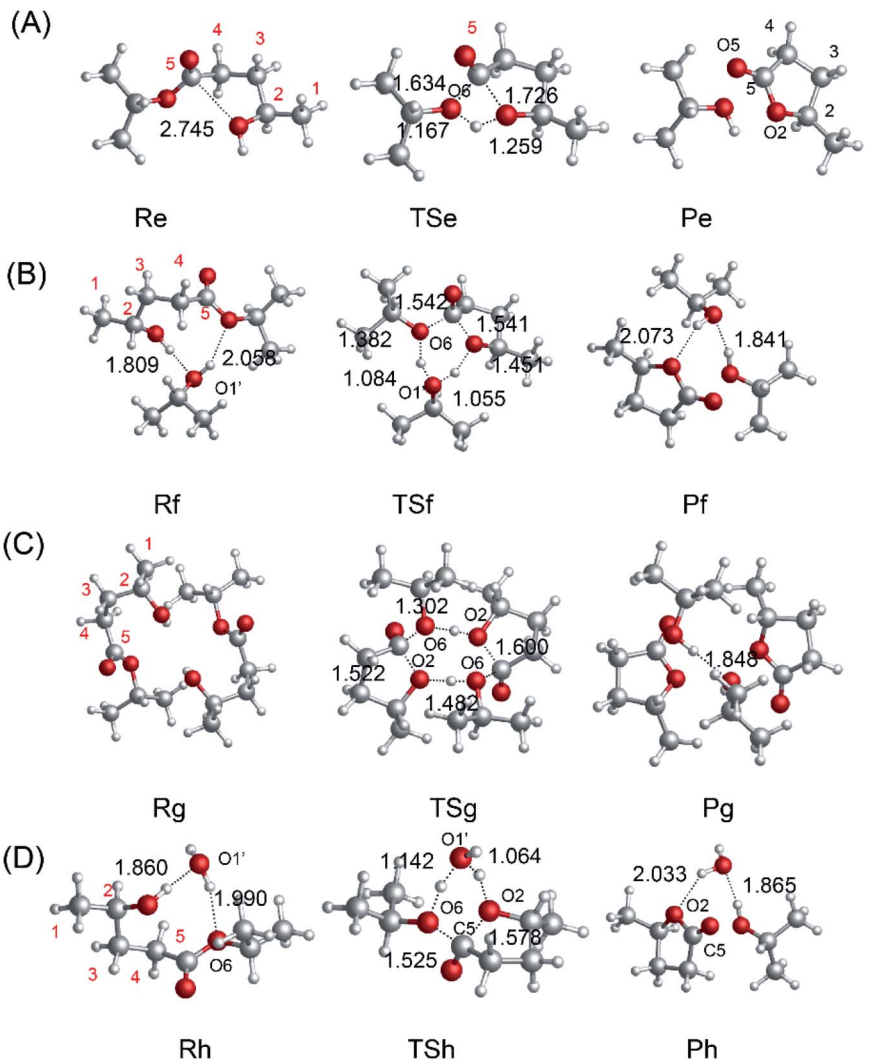

Fig. 6 Optimized geometries for the reactants, transition states, and products with (A) no catalyst, (B) i-PrOH, (C) 2HIPL, and (D) H_2O. The unit of chemical bond lengths is Å, 1 Å = 0.1 nm.

Table 3 Computed relative energies (kcal mol^{-1}) for the reaction of the ring-closure step catalyzed by different catalysts and the negative frequencies of the TSs

Catalyst	Activation energy [kcal mol^{-1}]	Reaction energy [kcal mol^{-1}]	Negative frequency of TS [cm^{-1}]
—	46.9	1.8	−1282.42
i-PrOH	37.4	2.4	−394.48
2HIPL	62.8	−2.9	−462.71
H_2O	39.4	−0.1	−782.58

reaction as a proton transfer mediator. To investigate the roles of the other catalysts, the corresponding reaction pathways were also studied, as shown in Fig. 6(B–D). Taking the reaction pathway catalyzed by i-PrOH as an example, the H transfers to the O of i-PrOH, and the H of the hydroxyl of i-PrOH transfers to O6 of 2HIPL. This process must overcome a 37.4 kcal mol^{-1} energy barrier, and is endothermic by about 2.4 kcal mol^{-1}. The oxygen of the catalysts plays the role of a proton shuttle to carry out the ring-closure reaction. Similarly to Rf-Pf (Fig. 6B), the ring-closure steps catalyzed by 2HIPL and H_2O were also calculated, and are shown in Fig. 6(C and D). As shown in Table 3, the barriers of the four kinds of ring-closure steps were calculated to be 46.9, 37.4, 62.8, and 39.4 kcal mol^{-1}, respectively. Comparing the activation energy of the different catalysts, their proton transfer ability follows the order i-PrOH > H_2O > 2HIPL. This means that i-PrOH plays a substantial role as a proton shuttle to promote the reaction.

To compare the catalytic effects of the Al-based catalysts, the reaction pathways were probed using DFT calculations. The structures of the different catalytic pathways are shown in Fig. 7. Some studies have reported that the bifunctional Lewis acid and Bronsted base sites of Al-based catalysts play an important role in sugar isomerization.[45,53] For R5 → P5 (Fig. 7A), the O5 of 2HIPL can coordinate with the Al^{3+} of $[Al(OiPr)_2(i\text{-}PrOH)]^{+1}$, and the O2–C5 bond is closed to produce GVL with a 37.1 kcal mol^{-1} energy barrier. This reaction is endothermic by about 1.1 kcal mol^{-1}. For R5′ → P5′ (Fig. 7B), the proton of O2H of 2HIPL transfers to the C2 of i-PrO$^{\bullet}$ coordinated with Al^{3+}, and the H2 of i-PrO$^{\bullet}$ migrates to the O6 of 2HIPL. The O2–C5 bond is closed to produce GVL with an 81.4 kcal mol^{-1} energy barrier. The reaction then proceeds *via* the formation of the product P5, which involves GVL, i-PrOH, and $Al(OiPr)_3$. This reaction is exothermic by about 1.6 kcal mol^{-1}. Al^{3+} located at a distance of about 0.1852 nm forms a hydrogen bond with the ketone oxygen in 2HIPL. These results show that $Al(OiPr)_3$ has poor proton transfer ability, and may not catalyze the ring-closure reaction in this way. In the other pathway of the ring-closure step catalyzed by $Al(OiPr)_3$ (R5″ → P5″) (Fig. 7C), the carbonyl O5 of 2HIPL is activated by coordination with $Al(OiPr)_3$. The H2 of the hydroxyl (2HIPL) migrates to O6, and a C5–O2 bond is formed *via* a four-membered ring TS. The energy barrier of this process is 40.1 kcal mol^{-1}. Comparing this value with the energy barriers of the processes catalyzed by the other catalysts discussed above, the Al-based catalysts are found to play an important role in the ring-closure reaction.

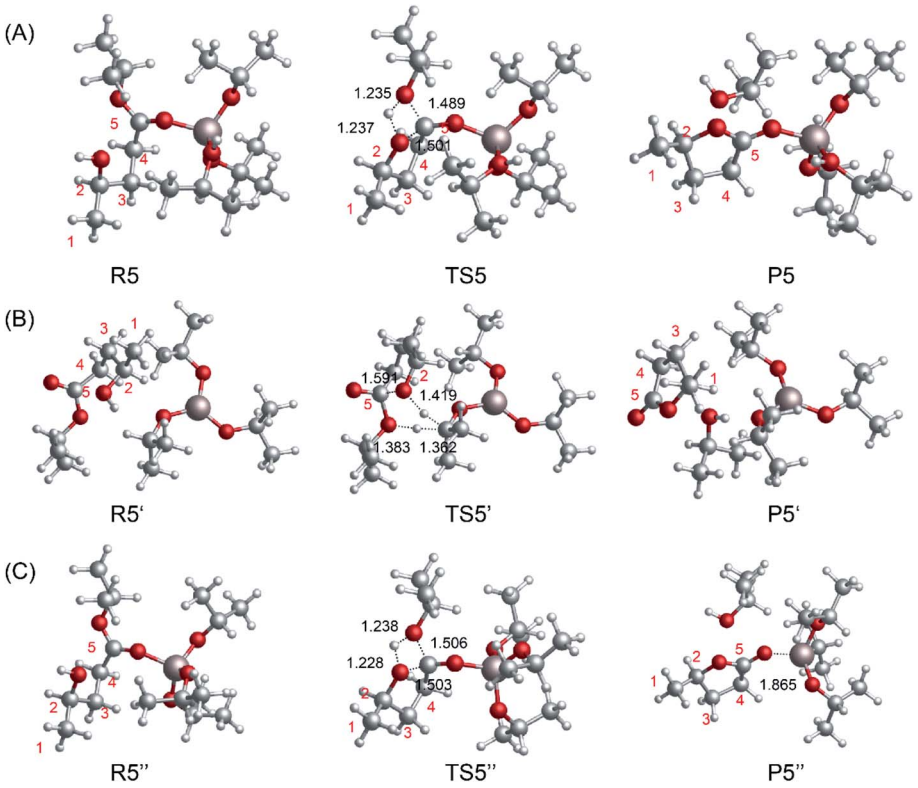

Fig. 7 Optimized geometries for the reactants, transition states, and products of the ring-closure step from 2HIPL to GVL catalyzed by the Al-based catalysts (A) $[Al(OiPr)_2(i\text{-}PrOH)]^{+1}$ and (B and C) $Al(OiPr)_3$. The unit of chemical bond lengths is Å, 1 Å = 0.1 nm.

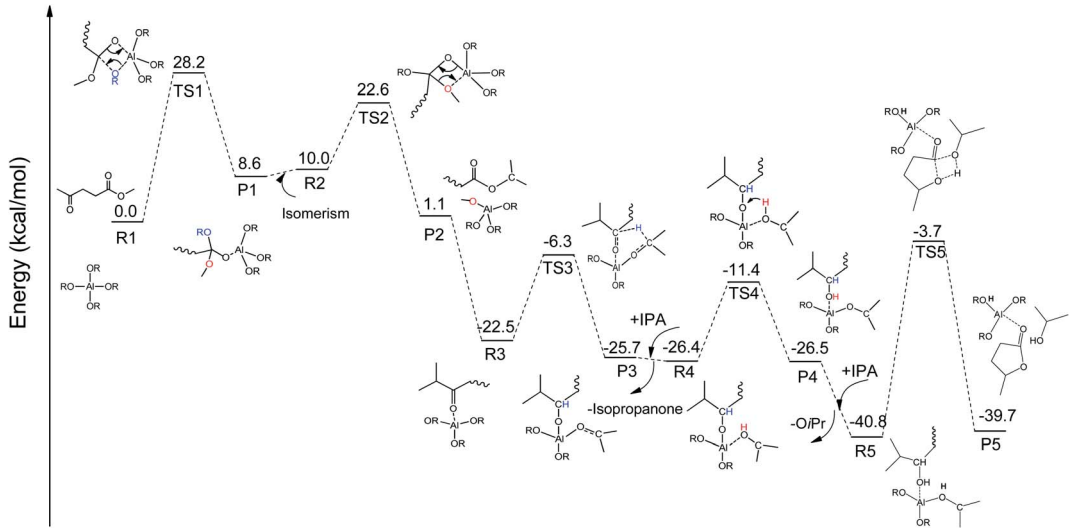

Fig. 8 The free energy profile of the formation of GVL from ML catalyzed by $Al(OiPr)_3$ in i-PrOH solvent with the relevant TSs noted corresponding to Scheme 2 (R═CH_3CHCH_3).

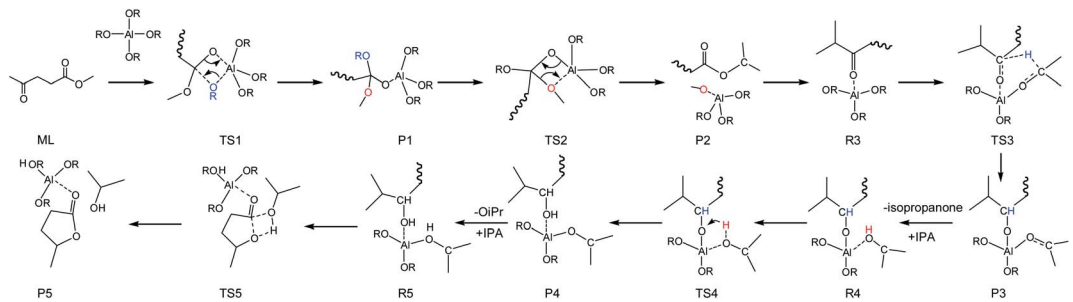

Scheme 2 Overall reaction pathway for the conversion of ML into GVL in i-PrOH solvent (R═CH_3CHCH_3).

3.4 Overall reaction process

To integrate all the basic steps, the lowest reaction pathways were combined. As shown in Fig. 8, the mechanism consists of three processes, namely, ester exchange, Meerwein–Ponndorf–Verley (MPV) hydrogenation, and the ring-closure step. The proposed reaction mechanism for the transformation of ML to GVL catalyzed by $Al(OiPr)_3$ in i-PrOH solvent is presented in Scheme 2. The ester exchange process involves two elementary steps. In the first step, $Al(OiPr)_3$ mainly interacts with the oxygen of ML to form the intermediate P1 *via* transition state TS1 with a barrier of 28.2 kcal mol^{-1}. The second step along the reaction coordinate is the isomerization of P1 to R2, with R2 being higher than P1 by about 1.4 kcal mol^{-1}. The methoxy group is then eliminated from R2, and transition state TS2 with a four-membered ring is formed. This process is just the reverse of the first step. Approximately 12.6 kcal mol^{-1} of energy is needed to cross the energy barrier. This reaction is exothermic by about 8.9 kcal mol^{-1}. The subsequent MPV process involves hydride transfer from the keto carbon of the $Al(OiPr)_3$ to the keto carbon of the intermediate isopropyl levulinate (IPL) (R3 → TS3) through transition state TS3 with an energy barrier of about 16.2 kcal mol^{-1}. In solution, the isopropanone will be replaced by an i-PrOH molecule, the i-PrOH in intermediate P3, to form the complex R4. This process (P3 → R4) is exothermic by only 0.7 kcal mol^{-1}. The release of the 2-hydroxy-isopropyl levulinate (2HIPL) (R4 → P4) requires a proton from the i-PrOH molecule. The protonation occurs *via* transition state TS4, which leads to the formation of 2HIPL and an isopropanone molecule (P4) with a 15 kcal mol^{-1} energy barrier. In the last process, the ring-closure step (R5 → P5), the O5 of 2HIPL can coordinate with Al^{3+} to catalyze the reaction. The rate-determining step is the ring-closure with a 37.1 kcal mol^{-1} energy barrier. The roles of $Al(OiPr)_3$ involve mainly coordination by the oxygen atoms of the reactants. A six-membered ring can be formed between $Al(OiPr)_3$ and IPL in the MPV reaction.

4. Conclusions

GVL is a promising renewable platform that can be produced from lignocellulose *via* LA/ML hydrogenation. In this paper, DFT calculations have been used to probe the details of the mechanism for the conversion of ML to GVL catalyzed by $Al(OiPr)_3$ in i-PrOH solvent. Comprehensive quantum chemical computations of the reaction *via* different pathways were

carried out, and there are three main processes (ester exchange, MPV hydrogenation, and the ring-closure step) involved. $Al(OiPr)_3$ mainly interacts with the oxygen of the carbonyl group ML to activate the reaction. In the ester exchange step, a four-membered ring transition state is formed between i-PrOH and ML, and two steps are required to complete this process. $Al(OiPr)_3$ can show a great catalytic effect *via* the formation of strong H-bonds, compared to when no catalyst is used. In the MPV hydrogenation reaction, IPL undergoes two proton additions with the catalyst $Al(OiPr)_3$ *via* a TS with six-centered-ring geometry. O5 of 2HIPL can coordinate with Al-based catalysts to reduce the barrier of the ring-closure step, which is rate-determining. The present theoretical study provides a clear elementary-step mechanistic profile of the transition from ML to GVL catalyzed by $Al(OiPr)_3$ and gives some basic guidance for the design of more efficient catalysts in the future.

Abbreviations

IPL	Isopropyl levulinate
2HIPL	2-Hydroxy-isopropyl levulinate
MPV	Meerwein–Ponndorf–Verley
GVL	γ-Valerolactone
LA	Levulinic acid
i-PrOH, IPA	Isopropanol alcohol

Conflicts of interest

There are no conflicts to declare.

Acknowledgements

This research was financially supported by the National Natural Science Foundation of China (No. 32071626) and the Research Fund for the Quzhou University (No. BSYJ202015 and BSYJ202113).

References

1 H.-J. Lee, W.-S. Lim and J.-W. Lee, *J. Ind. Eng. Chem.*, 2013, **19**, 2010–2015.
2 D. Kim, K. Lee and K. Y. Park, *J. Ind. Eng. Chem.*, 2016, **42**, 95–100.
3 M. J. Climent, A. Corma and S. Iborra, *Green Chem.*, 2014, **16**, 516.
4 J. Q. Bond, A. A. Upadhye, H. Olcay, G. A. Tompsett, J. Jae, R. Xing, D. M. Alonso, D. Wang, T. Zhang, R. Kumar, A. Foster, S. M. Sen, C. T. Maravelias, R. Malina, S. R. H. Barrett, R. Lobo, C. E. Wyman, J. A. Dumesic and G. W. Huber, *Energy Environ. Sci.*, 2014, **7**, 1500–1523.
5 K. Yan, Y. Yang, J. Chai and Y. Lu, *Appl. Catal., B*, 2015, **179**, 292–304.
6 C. E. Chan-Thaw, M. Marelli, R. Psaro, N. Ravasio and F. Zaccheria, *RSC Adv.*, 2013, **3**, 1302–1306.
7 Y. Yang, X. Wei, F. Zeng and L. Deng, *Green Chem.*, 2016, **18**, 691–694.
8 K. Yan, Y. Yang, J. Chai and Y. Lu, *Appl. Catal., B*, 2015, **179**, 292–304.
9 V. Fábos, M. Y. Lui, Y. F. Mui, Y. Y. Wong, L. T. Mika, L. Qi, E. Cséfalvay, V. Kovács, T. Szűcs and I. T. Horváth, *ACS Sustainable Chem. Eng.*, 2015, **3**, 1899–1904.
10 C. Xiao, T.-W. Goh, Z. Qi, S. Goes, K. Brashler, C. Perez and W. Huang, *ACS Catal.*, 2016, **6**, 593–599.
11 U. Omoruyi, S. Page, J. Hallett and P. W. Miller, *ChemSusChem*, 2016, **9**, 1–12.
12 X. Tang, H. Chen, L. Hu, W. Hao, Y. Sun, X. Zeng, L. Lin and S. Liu, *Appl. Catal., B*, 2014, **147**, 827–834.
13 A. M. R. Galletti, C. Antonetti, V. De Luise and M. Martinelli, *Green Chem.*, 2012, **14**, 688.
14 J. Song, L. Wu, B. Zhou, H. Zhou, H. Fan, Y. Yang, Q. Meng and B. Han, *Green Chem.*, 2015, **17**, 1626–1632.
15 H. Zhou, J. Song, H. Fan, B. Zhang, Y. Yang, J. Hu, Q. Zhu and B. Han, *Green Chem.*, 2014, **16**, 3870–3875.
16 X. Tang, H. Chen, L. Hu, W. Hao, Y. Sun, X. Zeng, L. Lin and S. Liu, *Appl. Catal., B*, 2014, **147**, 827–834.
17 A. Corma, M. E. Domine and S. Valencia, *J. Catal.*, 2003, **215**, 294–304.
18 T. Zhao, Z. Ju, Y. Zhang, L. Han and W. Xiao, *Chem. Eng. J.*, 2020, **390**, 124505.
19 M. Chia and J. A. Dumesic, *Chem. Commun.*, 2011, **47**, 12233–12235.
20 S. Wang, H. Huang, V. Dorcet, T. Roisnel, C. Bruneau and C. Fischmeister, *Organometallics*, 2017, **36**(16), 3152–3162.
21 S. Li, Y. Wang, Y. Yang, B. Chen, J. Tai, H. Liu and B. Han, *Green Chem.*, 2019, **21**, 770–774.
22 J. M. Nadgeri, N. Hiyoshi, A. Yamaguchi, O. Sato and M. Shirai, *Appl. Catal., A*, 2014, **470**, 215–220.
23 H. Zhou, J. Song, X. Kang, J. Hu, Y. Yang, H. Fan, Q. Meng and B. Han, *RSC Adv.*, 2015, **5**, 15267–15273.
24 H. Li, Z. Fang and S. Yang, *ACS Sustainable Chem. Eng.*, 2016, **4**(1), 236–246.
25 C. Zhang, Z. Huo, D. Ren, Z. Song, Y. Liu, F. Jin and W. Zhou, *J. Energy Chem.*, 2019, **32**, 189–197.
26 J. He, H. Li, Y.-M. Lu, Y.-X. Liu, Z.-B. Wu, D.-Y. Hu and S. Yang, *Appl. Catal., A*, 2016, **510**, 11–19.
27 P. Nandi, A. Solovyov, A. Okrut and A. Katz, *ACS Catal.*, 2014, **4**, 2492–2495.
28 M. J. Frisch, G. W. Trucks, H. B. Schlegel, G. E. Scuseria, M. A. Robb, J. R. Cheeseman, G. Scalmani, V. Barone, G. A. Petersson, H. Nakatsuji, X. Li, M. Caricato, A. V. Marenich, J. Bloino, B. G. Janesko, R. Gomperts, B. Mennucci, H. P. Hratchian, J. V. Ortiz, A. F. Izmaylov, J. L. Sonnenberg, D. Williams-Young, F. Ding, F. Lipparini, F. Egidi, J. Goings, B. Peng, A. Petrone, T. Henderson, D. Ranasinghe, V. G. Zakrzewski, J. Gao, N. Rega, G. Zheng, W. Liang, M. Hada, M. Ehara, K. Toyota, R. Fukuda, J. Hasegawa, M. Ishida, T. Nakajima, Y. Honda, O. Kitao, H. Nakai, T. Vreven, K. Throssell, J. A. Montgomery Jr, J. E. Peralta, F. Ogliaro, M. J. Bearpark, J. J. Heyd, E. N. Brothers, K. N. Kudin, V. N. Staroverov, T. A. Keith, R. Kobayashi, J. Normand, K. Raghavachari, A. P. Rendell, J. C. Burant, S. S. Iyengar, J. Tomasi, M. Cossi, J. M. Millam, M. Klene, C. Adamo,

R. Cammi, J. W. Ochterski, R. L. Martin, K. Morokuma, O. Farkas, J. B. Foresman and D. J. Fox, *Gaussian*, Gaussian, Inc., Wallingford CT, 2016.
29 H. Guernon and C. Y. Legault, *Organometallics*, 2013, **32**, 1988–1994.
30 Y. Zhao and D. G. Truhlar, *Theor. Chem. Acc.*, 2007, **120**, 215–241.
31 Y. Zhao and D. G. Truhlar, *Acc. Chem. Res.*, 2008, **41**, 157–167.
32 A. Schäfer, C. Huber and R. Ahlrichs, *J. Chem. Phys.*, 1994, **100**, 5829–5835.
33 S. Grimme, S. Ehrlich and L. Goerigk, *J. Comput. Chem.*, 2011, **32**, 1456–1465.
34 S. Grimme, J. Antony, S. Ehrlich and H. Krieg, *J. Chem. Phys.*, 2010, **132**, 154104.
35 Y. Zhao and D. G. Truhlar, *Theor. Chem. Acc.*, 2008, **119**, 525.
36 N. Y. Acelas and E. Flórez, *Adsorption*, 2018, **24**, 243–248.
37 F. Weigend and R. Ahlrichs, *Phys. Chem. Chem. Phys.*, 2005, **7**, 3297–3305.
38 C. Gonzalez and H. B. Schlegel, *J. Chem. Phys.*, 1991, **95**, 5853–5860.
39 A. V. Marenich, C. J. Cramer and D. G. Truhlar, *J. Phys. Chem. B*, 2009, **113**, 6378–6396.
40 R. Fu, T. Lu and F.-W. Chen, *Acta Phys.-Chim. Sin.*, 2014, **30**, 628–639.
41 J. S. Murray and P. Politzer, in *Encyclopedia of Computational Chemistry*, John Wiley & Sons, Ltd, 2002, DOI: DOI: 10.1002/0470845015.cca014.
42 A. Cesar Huppes da Silva, S. Claudino da Silva, E. L. Dall'Oglio, P. T. de Sousa and C. Alberto Kuhnen, *Fuel*, 2013, **104**, 379–385.
43 Y. Asakuma, K. Maeda, H. Kuramochi and K. Fukui, *Fuel*, 2009, **88**, 786–791.
44 Y. Jing, J. Gao, C. Liu and D. Zhang, *J. Phys. Chem. B*, 2017, **121**, 2171–2178.
45 Z. Ju, Y. Zhang, T. Zhao, W. Xiao and X. Yao, *ACS Sustainable Chem. Eng.*, 2019, **7**, 14962–14972.
46 S. Song, S. Yao, J. Cao, L. Di, G. Wu, N. Guan and L. Li, *Appl. Catal., B*, 2017, **217**, 115–124, S0926337317305015.
47 A. Corma, M. E. Domine, L. Nemeth and S. Valencia, *J. Am. Chem. Soc.*, 2002, **124**, 3194–3195.
48 S. H. Liu, S. Jaenicke and G. K. Chuah, *J. Catal.*, 2002, **206**, 321–330.
49 R. S. Assary, L. A. Curtiss and J. A. Dumesic, *ACS Catal.*, 2013, **3**, 2694–2704.
50 S. Grimme, S. Ehrlich and L. Goerigk, *J. Comput. Chem.*, 2011, **32**, 1456–1465.
51 D. Josa, J. Rodríguez-Otero, E. M. Cabaleiro-Lago and M. Rellán-Piñeiro, *Chem. Phys. Lett.*, 2013, **557**, 170–175.
52 R. Cohen, C. R. Graves, S. T. Nguyen, J. M. L. Martin and M. A. Ratner, *J. Am. Chem. Soc.*, 2004, **126**, 14796–14803.
53 S. Saravanamurugan, M. Paniagua, J. A. Melero and A. Riisager, *J. Am. Chem. Soc.*, 2013, **135**, 5246–5249.